Journal of Materials Chemistry A

Accepted Manuscript

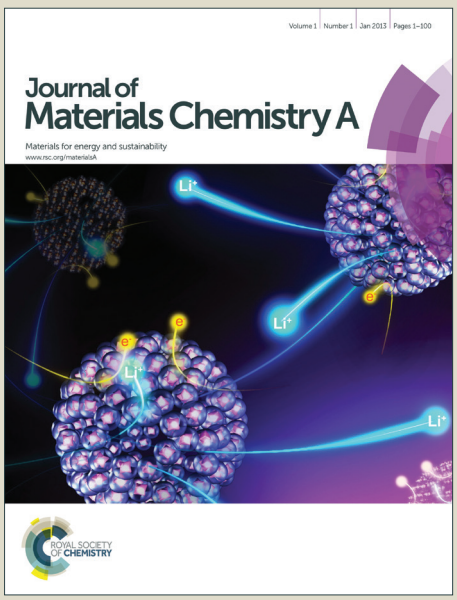

ROYAL SOCIETY OF CHEMISTRY

www.rsc.org/materialsA

Article type: Full Paper

Dye-Sensitized Solar Cells Based on Hierarchically Structured Porous TiO_2 Filled with Nanoparticles

*Zhenxuan Zhao [1], Guicheng Liu [1], Bo Li [2], Lixue Guo [1], Chengbin Fei [1], Yajie Wang [1], Lili Lv [2], Xiaoguang Liu [2], Jianjun Tian [1,2], Guozhong Cao *[1,3]*

Dr. Z. Zhao, Dr. G. Liu, L. Guo, C. Fei, Y. Wang, Prof. J. Tian, Prof. G. Cao
Beijing Institute of Nanoenergy and Nanosystems,
Chinese Academy of Sciences,
Beijing 100083, P.R.China
E-mail: gzcao@u.washington.edu

L. Bo, L. Lv, X. Liu, Prof. J. Tian
Advanced Material and Technology Institute,
University of Science and Technology,
Beijing 100083, PR China

Prof. G. Cao
Department of Materials and Engineering,
University of Washington,
Seattle, WA98195-2120, USA

Keywords: Dye-sensitized solar cell, three-dimensionally ordered macorporous structure, morphology, porous TiO_2

New morphology of TiO_2 photoanodes for N-719 dye-sensitized solar cells (DSCs) has been developed with enhanced power conversion performance. Strategies for the synthesis of hierarchically structured three-dimensionally ordered macroporous (HS-3DOM) TiO_2 with controlled macropore sizes (ca. 85 ~ 155 nm) by using well-arrayed polymethyl methacrylate with different diameters as well as two kinds of photoanode films based on hierarchically structured porous TiO_2 filled with nanopartcles have been demonstrated. DSCs based on the special TiO_2 photoanode with the macropore size of 105 nm exhibited a current density (J_{sc}) of 20.6 mA cm^{-2} and a high photo-to-electrical energy conversion efficiency (η) of 9.7%. This high power conversion efficiency is ascribed to the special morphology of TiO_2 photoanode

with high dye adsorption due to ordered and open structures, and also its light scattering and charge collection efficiency.

1. Introduction

The utilization of solar energy becomes increasingly important, as the fossil and mineral sources are limited and also the main source of environmental pollution. Dye-sensitized solar cells (DSCs) based on nanostructured semiconductor films as a type of photovoltaic devices have been considered as promising alternatives to silicon-based solar cells due to their low cost of materials and manufacturing[1]. However, improving their relatively low power conversion efficiency remains a big challenge confronting us since the highest efficiency of up to 13% compared with ~20% of silicon-based solar cells.[2] Photoelecrode, when loaded with dyes, as a component of DSCs is important due to its role as light harvester, charge generator, as well as electron collector [3]. The pore size, specific surface area, surface chemistry and defects, charge mobility, and charge recombination at the interface are all critical in achieving high power conversion efficiency [1d, 4]. Therefore, a lot of research including fabrication semiconductors with desired and unique micro and nanostructures as photoelecrodes, most commonly TiO_2 and ZnO_2, has been carried out to enhance the power conversion efficiency of DSCs.

In comparison with bulk material, nanocrystalline photoelecrodes can adsorb more dye molecules due to their high specific surface area [5]. However, the existence of numerous boundaries in nanocrystalline films would unavoidably increase interfacial charge recombination and reduce the charge mobility. Nanowires, nanorods, or nanotubes with one-dimensional structures in the nature of single crystal form would provide direct pathways for efficient electron transport to reduce charge recombination at the interface or grain boundaries [3a, 6]; however, one dimensional nanostructures suffer from a relatively low specific surface area to ensure sufficient dye loading. Photoelectrodes with hierarchical structures exhibit

many advantages in enhancing power conversion efficiency of DCSs [7], such as possessing large specific surface area and effective light scattering, accommodating sufficient dye loading, facilitating electron transport and electrolyte diffusion due to the compact packing of the nanocrystallites and the relative open structure [4]. Hierarchical structures, which have been studied in the field of DSCs, include spherical/nanorod/ core-shell aggregates[7a, 7c, 7f, 8].

Three-dimensionally ordered macroporous (3DOM) TiO_2 have attracted particular attention in photocatalyst [9] and photovoltaic [10] application due to its high surface area, novel optical and electronic abilities, interconnected porosity, extremely uniform size, periodic distributions of pores. 3DOM TiO_2 can be fabricated by using monodisperse latex spheres as hard template [11]. However, overlayers on top of the 3DOM architecture destroy the quality of 3DOM TiO_2 due to the air- and moisture-sensitve for titanium alkxoxides. Therefore many synthetic methods such as sandwich-vacuum method[12] and opal infiltration method[13] by using polystyrene as template have been adopted. Herein, a simple method using self-assembled polymethyl methacrylate (PMMA) spheres as templates and tetraisopropyl titanate solution with moisture stability was used to fabricate high quality hieratically structured 3DOM TiO_2 in ambient. After the removal of PMMA spheres and subsequent heat treatment, a kind of hierarchically structured porous TiO_2 filled with nanoparticles has been studied as photoanode in DSCs and the impacts of such hierarchical structure on dye loading, light scattering and charge transport properties, and consequent power conversion efficiency have been studied and discussed.

2. Results and Discussion

Figure 1(a~e) shows the SEM images of as-fabricated hierarchically structured three-dimensionally ordered macroporous TiO_2 after the removal of PMMA templates. All of these samples exhibited excellent three-dimensionally ordered macroporous architectures. It indicates that the TiO_2 with three-dimensionally ordered macroporous structures could be

successfully fabricated with regularly packed PMMA microspheres, and their qualities were better than that of three-dimensionally quasi-ordered macropore TiO_2 prepared through poly(vinyl alcohol) gelated crystalline colloidal array.[14] We synthesized four samples with macropore diameters of ca. 155, 115, 105, and 85 nm. In Figure 1(f), the positions of XRD lines for all the samples were the same and could be well indexed to the standard anatase TiO_2 XRD pattern (JCPDS PDF no. 78-2486). Therefore, it can be deduced that all these samples possessed anatase crystal structure.[15] It have been reported that the macropore diameters could be controlled by the size of the PMMA microspheres.[16] The SEM images of hard templates shown in **Figure S1** of Supporting Information exhibited the well-arrayed PMMA microspheres templates with 280, 220, 200, and 150 nm in diameter and their corresponding pore sizes in TiO_2 samples are 155, 115, 105, and 85 nm, respectively. The macropore sizes in 3DOM TiO_2 samples are 55% smaller than diameters of PMMA microspheres. It can be easily understood that after the removal of PMMA microsphere through decomposition and oxidation during thermal treatment, loosely assembled TiO_2 nanoparticles would go through slight adjustment and partial sintering and densification leading to the shrinkage of void spaces. What is more, the surfaces of all these 3DOM TiO_2 were rough observed from SEM images (Figure 1(a~e)). Under TEM observation (**Figure 2**), the detailed morphological structures can been seen that the frameworks of these TiO_2 samples with 3DOM architectures comprised by nanoparticles of 7 ~ 35 nm. High-resolution TEM (HR-TEM) image in Figure 2(f) shows that the lattice space (*d*) of nanoparticles were 0.35 nm and matches nearly exactly to the theoretical value (3.5165 Å) of (101) plane of anatase TiO_2 crystalline.

The nitrogen adsorption-desorption isotherms of the TiO_2 samples are shown in **Figure S2**(A). According to the IUPAC classification, the adsorption isotherms can be classified as II isotherms.[17] An adsorption-desorption hysteresis loop with a H3 typeis observed in the relative pressure (p/p_0) range of 0.8-1.0,[17a] which does not clearly exhibit any adsorption

plateau at relative pressures close to saturation, suggests the fact of macropore existence,[17a] that was identical with the macroporous structres observed from the SEM images. What is more, the low-pressure portion of the almost linear middle section of the isotherm, which is attributable to the unrestricted mono- or multilayer adsorption, indicates the existence of macropores.[18] Futhermore, there are initial jumps of adsorption isotherms observed from the low-pressures section in Figure S2(C). It represents the existence micropores.[19] The pore size distribution curves calculated by BJH method were shown in Figure S2(B). All of samples exhibited two pore size distributions: one broad peak centered at 29~45 nm and one narrow peak centered at 2~10 nm and, which can be due to the macropores generated by the removing PMMA spheres and micropores which are the gaps between adjacent packed nanoparticles, respectively. This result was in good agreement to that of adsorption-desorption isotherms and the observation from TEM images. **Table S1** lists their BET surface areas and pore volumes. It was found that the surface areas and pore volumes were increased in the range of 46.1~114.5 $m^2 g^{-1}$, 0.25~0.82 $cm^3 g^{-1}$, respectively, with the decreasing macropore size of HS-3DOM TiO_2 samples from 155 nm to 85 nm. Contrarily, a decline trend was observed on the values of surface area/pore volume from 184 cm^{-1} to 140 cm^{-1} while the macropore sizes were decreased.

The pastes based on HS-3DOM TiO_2 were obtained by the treatments described in experimental section. The cross-section SEM images of photoanode based on Ti-155 were shown in **Figure 3**(a), the thickness of the porous TiO_2 layer was about 9 μm and the compact layer, which was used as hole-blocking layer to prevent direct contact between the FTO and electrolyte, was about 0.3 μm. A configuration of a full DSC-device was illustrated in Figure 3(b). From magnifying images of Ti-155 layer showing in Figure 3(c,d), it can be observed that HS-3DOM TiO_2 particles had been break up into small particles. However, they did not lose their three-dimensionally ordered skeletal structure completely. These splitting particles

mixed together randomly to form a disordered status. Observation from the images of Ti-85 layer in Figure 3(f, g) can be found that many nanoparticles were covered on the surface of particles with 3DOM structures. The status was different from the former one. We deduced that small particles with 3DOM architectures and nanoparticles, which can be break up from their mother particles easily, could generate after the same experimental treatments in all samples. As for the Ti-155 paste, some nanoparticles could be filled into macropores as described in Figure 3(e). So, it is hard to find nanoparticles from the SEM image of Ti-155 layer in Figure 3(d). Whereas, as for the Ti-85 pastes, macropores with smaller size could not let nanoparticles filled in, which have to stay out of pores as illustrated in Figure 3(h). There are many factors for these two kinds of special morphologies pastes facilitate the performance of DSCs. For one thing, as depicted in the schemes (Figure 3(e,h)), lots of nanocrystallites breaking up from larger particles can help contributing to enhance their surface area which adsorbed N719 dye for light harvesting. Secondly, ordered structure is beneficial to photogenerated charge transportation as shown in Figure 3(e). Lastly, the porous TiO_2 possess the relatively open structure which allows I^-/I_3^- electrolyte to completely wet its surface and facilitate electrolyte diffusion.

A strategy for preparing HS-3DOM TiO_2 with tunable macropore sizes has been developed by using crystalline colloidal array PMMA photonic crystal microsphere packed in the form of face-centered-cubic structure as template shown in **Figure 4**(a) and tetrasopropyl titanate with PEG-400 and HNO_3 in EtOH solution as Ti precursor. The first step was dipping the well-arrayed PMMA powder (Figure 4(a)) into the Ti precursor solution for four hours. Then, residual solution have been removed and the left solution have been absorbed into the voids of hard template by the force of capillary pressure as described in Figure 4(b). The EtOH or absorbing water from air can be removed through drying at ambient temperature and calcination at 160 ^oC for 3 h, which was confirmed by TGA/DSC measurement (**Figure S3** in

Supporting Information). Then, the micelle will rearrange during the removal of EtOH solution due to the density of the micro-emulsion getting to the critical density shown in Figure 4(c). In this state, organic molecule (PEG-400, $(CH_3)_2CHO$) becomes an inhibiter to wrap up Ti compounds, which was mainly $TiO(OH)_2$ described in Figure 4(c). After calcination at 550 ^oC in air atomsphere, organic molecules including PEG-400, $(CH_3)_2CHO$, and PMMA were removed thoroughly, and $TiO(OH)_2$ was decomposed turn into anatase TiO_2 with HS-3DOM structures aggregated nanoparticles shown in Figure 4(d) indentified to the TGA/DSC measurement. According to different macropore size of HS-3DOM TiO_2, the hierarchically structured porous TiO_2 layers present two kinds of morphologies as shown in the HR-SEM images (Figure 4(k,l)). Their big particles could break into many pieces when subjected to unltrasonication and still maintain 3DOM architectures (Figure 4(f,i)). As for the Ti-155, Ti-115, and Ti-105 pastes which macorpore sizes larger than 105 nm (Figure 4(e)), big particles blend together randomly and splitted nanoparticles could get into the macropores of big pieces, which were large enough to let these nanopraticles fall into them (Figure 4(g)). As for the Ti-85 pastes, most nanoparticles were blocked at the surface of macroporous particles due to its smaller macropore sizeas observed in Figure 4(I).

Figure 5 shows the current density-voltage (J-V) curves of DSCs based on hierarchically structured porous TiO_2 filled with nanoparticles. The power conversion efficiency of these devices increased from 7.08% to 9.74% along with the decreasing macropore size of porous TiO_2 layers from 155 nm to 105 nm listed in a table inserted in Figure 5. In particular, the solar cell device based on Ti-105 exhibited a short-circuit current density (J_{sc}) of 20.68 mA cm^{-2} and energy conversion efficiency (η) of 9.74%. Compared to the DSC device base on Ti-105 film, devices based on Ti-155 and Ti-115 had J_{sc} and η values of 16.35 mA cm^{-2}, 7.07%, and 19.92 mA cm^{-2}, 8.17%, respectively, With the lowest power conversion efficiency of 6.15% found in DSC based on Ti-85 film. Their open-circuit voltages V_{oc} (718±11 mV)

determined by the difference between the Fermi levels of the oxide semiconductor and the redox potential of the electrolyte were almost the same in all of the hierarchically structured porous TiO_2 devices.[20] Their fill factors FF, which were imitated with the geometry structure and the transport mechanism of carries in each individual cell,[20] varied from 57.9% to 64.9%.

The amount of adsorbed dye on each cells were investigated; **Table 1** shows that the amounts of adsorbed dye on hierarchically structured porous TiO_2 increased from 238 nmol cm^{-2} to 264 nmol cm^{-2} with reduced macropore sizes in Ti-155, Ti-115, and Ti-105 photoanodes, and dropped dramatically to 233 nmol cm^{-2} on the Ti-85 one. In order to investigate the amount of dye adsorption was alter with the changing macropore sizes in our synthesized photoanode films, the surface area and pore volume of all powders obtained from drying pastes, which were used to assembled as photoanodes, had been detected by nitrogen sorption isotherms and calucated by BET and BJH methods, respectively. Observed from the texture parameters listed in Table 1, the values of surface area were become larger than these of their corresponding samples before treatment (Table S1). The total area per square centimeter of photoanode *A* can be deduced by the value of surface area (a) and pore volume (v_p). A given volume v of per gram porous material includes the volume of 1 g bulk material and the total one of pores in 1 g porous material, just as pore volume (v_p) , can be calculated as **Equation 1**:

$$v\ (\mathrm{cm}^3) = \frac{1}{\rho_{\mathrm{bulk}}} + v_{\mathrm{p}} = 0.257 + v_{\mathrm{p}} \qquad (1)$$

Where ρ_{bulk} = 3.893 cm^3 g^{-1} is the density of bulk anatase TiO_2, Therefore, the total surface area per square centimeter of photoanode *A* can be calculated by the following **Equation 2**.

$$A\ (\mathrm{cm}^2) = \mathrm{V}\,\rho\,a = \frac{9.5 \times 10^{-4} a}{0.257 + v_{\mathrm{p}}} \qquad (2)$$

Where *d* is the thickness of photoanode film. It was about 9.5 μm in our photoanodes. All of the data were listed in Table 1. The result valve of *A* increased in the range of Ti-155<Ti-115<Ti-105 from 1.076×10^{17}nm^2 to 1.143×10^{17}nm^2 and dropped to 1.045×10^{17}nm^2 in the Ti-85 sample. It has been reported that the per 1 nm^2 TiO_2 can be filled by 1.95 N719 molecules.[1a] Therefore, we can calculate the ideal amount of adsorbed dye in 1 cm^2 active area of devices varied from 338.6 to 358.8 nmol cm^{-2} and listed in Table 1. Apparently, the amount of adsorbed dye were ca. 70% of ideal ones and have the same sequence with their J_{sc} values, which were higher than that (7 ~ 10 mA cm^{-2}) of DSCs based on TiO_2 nanoparticles with the same dye coverage[1a]. Furthermore, the as-assemblied solar cell based on Ti-105 with 264 nmmol cm^{-2} dye-loading performed more better than the one based on three-dimenstionally array of TiO_2 nanotubes with near the same amout of adsorbed dye (260 nmmol cm^{-2}). [21]

Diffused reflectance and transmittance of hierarchically structured porous TiO_2 layers with and without dye adsorption was measured by UV-vis spectrophotometer to character their light scattering, which is an important factor influencing the performance of DSCs. It is widely known that the ideal light scattering activities of the photoanode should have a higher diffuse reflectance and lower diffuse transmittance. In **Figure 6**(A,B), the diffuse reflectance of bare porous TiO_2 layer was in the sequence of Ti-155 < Ti-115 < Ti-105 in the range of 400~800 nm, corresponding to their transmission in the order of Ti-155 > Ti-115 > Ti-105. The increased reflectance and suppressed transmission along with the decreasing macropore sizes in Ti-155, Ti-115, and Ti-105 films may be ascribable to sufficient light scattering due to their porous architectures.[22] However, it is interesting that the reflectance of Ti-85 did not continue to rise with decreasing macropore size and became weaker than the one of Ti-155 in the range of 500~800 nm. This result may be ascribable to their morphologies. Furthermore, the diffused reflectance and transmission of dye-adsorbed porous TiO_2 films have been

investigated and shown in Figure 6(C,D). Apparently, they have the same sequences in the reflectance and transmission abilities in the dye-absorbed porous TiO_2 layer according to their corresponding layers without dye loading.

The transport and interfacial transfer of electrons in DSCs can be investigated using intensity modulated photocurrent and photovoltage spectroscopy (IMPS/IMVS). The effective electron transport (τ_t) and electron lifetime (τ_r) can be obtained from IMPS/IMVS measurements by adjusting light intensity to determined open-circuit voltage, respectively. The data can be calculated through the following **Equation 3** and **4:**[23]

$$\tau_t = 1/2\pi f_t \quad (3)$$

$$\tau_r = 1/2\pi f_r \quad (4)$$

f_t and f_r are the characteristic frequency minimums of the IMPS and IMVS imaginary components, respectively. **Figure 7**(A,B) shows the τ_t and τ_r plots as a function of the open-circuit voltage for DSCs based on Ti-155, Ti-115, Ti-105, and Ti-85. Obviously, the τ_t of all devices were decreasing tenderly with the increasing voltage, which can be attributed to the trapping/detrapping for electron with shallower levels due to the deep traps filled by more photoelectrons at higher voltage. As for the τ_r exhibited the downward tendency, ascribable to the increase in the electron recombination rate in higher voltage. Furthermore, the τ_t and τ_r of these DSCs were increasing slightly in the sequence of Ti-155 < Ti-115 < Ti-105 < Ti-85, suggesting that the electron transport rate and electron recombination rate decreased a little with the increasing macropore size in hierarchically structured porous TiO_2. It is said that the electron recombination could enhance with the increasing surface area/pore volume due to the rising surface defects that result to more charge trapping.[24] However, the electron recombination rate of DSCs based on Ti-85 which possessed the largest surface area/pore volume (140 cm^{-1}) listed in Table S1 was the lowest compared by other devices. This maybe due to the special geometry architecture of the photoelectrodes. Furthermore, electron

collection efficiency (η_{col}) can be estimated using of τ_t and τ_r according to the given **Equation 5**: [25]

$$\eta_{col} = \frac{J_{sc}}{J_{inj}} = \frac{J_{sc}}{J_{sc} + J_r} = \frac{\frac{1}{\tau_t}}{\frac{1}{\tau_t} + \frac{1}{\tau_r}} = 1 - \frac{\tau_t}{\tau_r} \quad (5)$$

Where J_{inj} is the electron-injection current density from the excited dye to TiO_2 and J_r is the recombination-current density. Figure 7(C) shows the η_{col} plots as a function of voltage from 0.18 V to 0.90 V. The η_{col} of the DSCs were increased in the order of Ti-85 < Ti-155 < Ti-115< Ti-105 with the same arrange of J_{sc} which are proportional to η_{col} as depicted in Equation 5.

The electrochemical impedance spectroscopy (EIS) analyses were measured to study the charge-transfer property in the DSCs based on hierarchically structured porous TiO_2 as photoelecrodes; the Nyquist plots of the EIS results including various resistance elements for these DSCs devices were shown in Figure 7(D) and Table 2. The equivalent circuit can be interpreted by resistance-capacitance elements inserted in Figure 7(D). The impedance plots of a DSC device have two semicircles in the Nyquist diagram as shown in Figure 7(D). The first semicircle at high frequencies (R_t) is generated by the redox reaction at the platinum counter electrode/electrolyte interface; another one at lower frequencies (R_{ct}) can be ascribable to the electron transfer between oxide/electrolyte interface and is equivalent to the recombination resistance;[26] the ohmic resistance R_s is caused by sheet resistance of the FTO glass.[8] It is obviously that the R_s and R_t of the DSCs were almost 6.92 and 2.45 Ω cm^2, respectively, and the extents of the numerical values variation were very small; the R_{ct} of all DSCs based on hierarchically structured porous TiO_2 was increased from 10.97 to 16.55 Ω cm^2 with the decreasing macorpore size of photoelecrodes. It means that the ohmic resistance and the redox reaction resistance at counter electrode of these DSCs were almost equal; the

charge recombination capabilities of these DSCs reduced with the decreasing macorpore size of hierarchically structured porous TiO_2 in the order of Ti-155 < Ti-115 < Ti-105 < Ti-85, whose changing trends were same to the open-circuit voltage variations of these DSCs. This results are consistent with the result obtain by J-V test (Figure 5) and IMVS study (Figure 7(B)).

3. Conclusions

Herein, a kind of TiO_2 photoanode with hierarchically structure pores filled with nanoparticles had been prepared by using hierarchically structured three-dimensionally ordered macroporous (HS-3DOM) TiO_2. In this paper ,we reported the synthesis method of HS-3DOM TiO_2 with different macropore sizes (155, 115, 105, and 85 nm) by using well-arrayed PMMA microspheres. The results of their physical characterizations showed that micropores and macropores coexisted in all the HS-3DOM TiO_2 samples with anatase crystal structure. hierarchically structure porous TiO_2 layers fabricated from HS-3DOM TiO_2 exhibited two kinds of morphologies, including ones of nanoparticles filled into macropores and one of nanoparticles blocked on the surface of macropores. The highest energy conversion efficiency of these devices was achieved at 9.44% on the DSC device based on Ti-105 with the highest short-circuit current density (J_{sc} = 20.76 mA cm^{-2}), which was the main factor influencing the efficiency due to the little change in open-circuit voltages V_{oc}. The amount of dye adsorption (101.5 ~ 114.8 mmol cm^{-2}), which was affected by surface area, pore volume, and thickness of photoanode, affected the DSCs short-circuit current density and was just in the same sequence of J_{sc} (Ti-85 < Ti- 155 < Ti-115 < Ti-105). What's more, the light scattering capability of photoanode, another important factor influencing the J_{sc}, exhibited the same sequence, too. The IMPS/IMVS results showed that the effective electron transport τ_t and electron lifetime τ_r increased in the order of Ti-155 < Ti-115 < Ti-105 < Ti-85, that was

proved by EIS. The efficiencies were also affected by the electron collection efficiency η_{col} which obtained by τ_t and τ_r.

Experimental Section

Synthesis of highly ordered PMMA colloidal crystal microspheres: The PMMA colloidal crystal microspheres with different diameters were synthesized using emulsifier-free emulsion polymerization approach by adjusting the using amount of $K_2S_2O_8$ and MMA.[16] A three-necked round-bottomed alaskite reactor filled with deionized water equipped with a magnetic stirrer was heated under 70 ^oC. A water-cooling condenser with the upper end connected to a wash-bottle containing ethanol solution was fixed to the reactor. A certain amount of methyl methacrylate monomer was poured into the reactor under 70 ^oC. After stirring thoroughly with water, $K_2S_2O_8$ as polymerization inhibitor was added into the reactor under stirring. Then, a milky white solution containing PMMA could be generated after 40 min. The reaction could be stopped by dropping the solution into cool deionized water. The highly ordered PMMA arrays could be acquired by centrifugation of the PMMA-containing liquid. All of the experimental processes must be protected by N_2 atmosphere. Herein, PMMA with 280, 220, and 200 nm of macropore diameters could be fabricated by using 115 ml of MMA in 1300 ml of water with 0.4, 0.2, and 0.1 g of $K_2S_2O_8$, respectively. PMMA with 150 nm of diameter could be obtained by using 30 ml of MMA in 330 ml of water with 0.2 g of $K_2S_2O_8$.

Synthesis of hierarchically structured three-dimensionally macroporous TiO_2 pastes: The titanic precursor was tetraisopropyl titanate ($Ti(OC_4H_8)_4$)solution (40 vol%) containing 2 mol/L concentrate nitric acid and 0.2 mol/L PEG-400 additives. The total amount of the precursor was 25 mL. The obtained well-arrayed PMMA templates were impregnated into the above precursor solution for 4 hours at room condition. After filtering the excessive liquid, the obtained samples were dried in a desiccator. Then, the hierarchically structured three-dimensionally ordered macroporous (HS-3DOM) TiO_2 samples could be obtained by

calcinated the precursor in air at a ramp of 1 ^{o}C/min from room temperature to 200 ^{o}C and 550 ^{o}C and kept at these temperatures for 3 h. The macropore size of HS-3DOM TiO_2 depended on the diameter size of PMMA microsphere. Herein, the as-fabricated HS-3DOM TiO_2 samples with macrorpore size of ca. 155, 115, 105, and 85 nm were fabricated through using PMMA microspheres with 280, 220, 200 and 115 nm of diameters, respectively, and can be noted as Ti-155, Ti-115, Ti-105, and Ti-85 according to their macropore sizes. The HS-3DOM TiO_2 pastes could be obtained via the following method: add 0.05 g of the as-obtained HS-3DOM TiO_2 powders into 0.4 mL of ethanol solution (50 %). The mixtures were sequentially treated by ultrasonic treatment with 60 Hz for 1 min and mixing for 1 min. Both of these two steps should be operated strictly. The result pastes could be obtained after 5 cycles.

Assembly of dye-sensitized solar cells: FTO-coated glass were used as substrate after washed subsequently with diluted cleaning detergent solution, deionized water, acetone, and ethanol. A liquid admixture containing 1 mL tetraisopropyl titanate, 0.5 mL ethanolamine, and 5 mL ethylene glycol monomethyl ether was spin-coated onto the clean substrates at 3000 rpm. A compact TiO_2 layer was formed after drying at 160 ^{o}C for 1 h and sintering at 500 ^{o}C for 1 h. It was used to prevent direct contact between the substrate and the electrolyte. The doctor-blade technique was used to prepare porous TiO_2 layer onto the compact layer. After thermal treatment under 125 ^{o}C for 1 h and 450 ^{o}C for 2 h, the result photoanode was immersed in 0.3 mM N719 absolute ethanol solution for 72 h, followed by cleaning with absolute ethanol. The chemically platinized silicon wafer (Co. Ltd. PV-Tech) was used as counter electrode. The electrolyte (OPV-AN-I, Co. Ltd. PV-Tech) was sandwiched by a sensitized TiO_2 electrode and a counter electrode with two clips.

*Characterization***:** The morphology, crystal structure, and surface area of the as-fabricated HS-3DOM TiO_2 samples were characterized by Scanning Electron Microscopy (SEM,

Gemini Zeiss Supra 55), High-resolution Transmission Electron Microscopy (HR-TEM, JEOL-2010), X-Ray Diffraction (Bruker/AXS D8 Advance), and nitrogen sorption isotherms (Micrometeritic 2020), respectively. Current-Voltage behaviors were characterized under simulated AM 1.5 sunlight with an output power of 100 mW cm^{-2}, which was calibrated by a NREL-calibrated Si solar cell, generated by a solar simulator (91192, 1kW Xe lamp, Oriel). The solar cells were masked with a metal aperture to define the active area of 0.126 ± 0.002 cm^2. UV-Vis-NIR spectrophotometer (Shimadzu, UV-3600) was used to analyze the diffuse reflectance and diffuse transmittance of the TiO_2 films. Intensity-modulated photovoltage spectroscopy (IMPS) at short circuit and intensity-modulated photocurrent spectroscopy (IMVS) at open circuit were measured on an electrochemical workstation (Zahner, Zenium) with a frequency response analyzer under blue light emitting diodes (457 nm) driven by a Zahner (PP211) source supply as modulated light source. Electrochemical impedance spectra (EIS) were measured at open circuit under dark condition. Impedance data were fitted using Zview 3.3e software (Scribner Associates, Inc.).

Supporting Information

Supporting Information is available from the Wiley Online Library or from the author.

Acknowledgements

This work was supported by the "thousands talents" program for pioneer researcher and his innovation team, China. This work was also supported by the National Science Foundation of China (51374029), Program for New Century Excellent Talents in University (NCET-13-0668), Fundamental Research Funds for the Central Universities (FRF-TP-14-008C1) and China Postdoctoral Science Foundation (2014M550675).

Received: ((will be filled in by the editorial staff))
Revised: ((will be filled in by the editorial staff))
Published online: ((will be filled in by the editorial staff))

[1] a) M. Grätzel, *J. Photoch. Photobio. C.* **2003**, *4*, 145; b) Q. Zhang, C. S. Dandeneau, X. Zhou, G. Cao, *Adv. Mater.* **2009**, *21*, 4087; c) Q. Zhang, G. Cao, *Nano Today* **2011**, *6*, 91; d) Q. Zhang, E. Uchaker, S. L. Candelaria, G. Cao, *Chem. Soc. Rev.* **2013**, *42*, 3127.

[2] a) S. Mathew, A. Yella, P. Gao, R. Humphry-Baker, B. F. E. Curchod, N. Ashari-Astani, I. Tavernelli, U. Rothlisberger, M. K. Nazeeruddin, M. Graetzel, *Nat. Chem.* **2014**, *6*, 242; b) Q. Wang, S. Ito, M. Graetzel, F. Fabregat-Santiago, I. Mora-Sero, J. Bisquert, T. Bessho, H. Imai, *J. Phys. Chem. B* **2006**, *110*, 25210; c) G. W. Crabtree, N. S. Lewis, *Phys. Today* **2007**, *60*, 37; d) M. Grätzel, *Inorg. Chem.* **2005**, *44*, 6841.

[3] a) B. Oregan, M. Grätzel, *Nature* **1991**, *353*, 737; b) D. B. Kuang, S. Ito, B. Wenger, C. Klein, J. E. Moser, R. Humphry-Baker, S. M. Zakeeruddin, M. Grätzel, *J. Am. Chem. Soc.* **2006**, *128*, 4146; c) C. J. Barbe, F. Arendse, P. Comte, M. Jirousek, F. Lenzmann, V. Shklover, M. Grätzel, *J. Am. Ceram. Soc.* **1997**, *80*, 3157.

[4] Q. Zhang, G. Cao, *J. Mater. Chem.* **2011**, *21*, 6769.

[5] a) M. Grätzel, *Nature* **2001**, *414*, 338; b) S. Yang, *Abstracts of Papers of the American Chemical Society* **2012**, *243*.

[6] M. Law, L. E. Greene, J. C. Johnson, R. Saykally, P. D. Yang, *Nat. Mater.* **2005**, *4*, 455.

[7] a) Z. Nie, X. Zhou, Q. Zhang, G. Cao, J. Liu, *Scie. Adv. Mater.* **2013**, *5*, 1750; b) R. Gao, Z. Liang, J. Tian, Q. Zhang, L. Wang, G. Cao, in *Fullerenes, Nanotubes, and Carbon Nanostructures - 221st Ecs Meeting,* **2013**, pp. 127; c) R. Gao, J. Tian, Z. Liang, Q. Zhang, L. Wang, G. Cao, *Nanoscale* **2013**, *5*, 1894; d) J. Xi, Q. Zhang, D. Myers, Y. Sun, G. Cao, *J. Nanophotonics* **2012**, *6*; e) J. Lin, Y.-U. Heo, A. Nattestad, Z. Sun, L. Wang, J. H. Kim, S. X. Dou, *Sci. Rep.* **2014**, *4*; f) J. Lin, A. Nattestad, H. Yu, Y. Bai, L. Wang, S. X. Dou, J. H. Kim, *J. Mater. Chem. A* **2014**, *2*, 8902.

[8] K. Park, Q. Zhang, B. B. Garcia, G. Cao, *J. Phys. Chem. C* **2011**, *115*, 4927.

[9] J. I. L. Chen, G. von Freymann, V. Kitaev, G. A. Ozin, *J. Am. Chem. Soc.* **2007**, *129*, 1196.

[10] a) S. Nishimura, N. Abrams, B. A. Lewis, L. I. Halaoui, T. E. Mallouk, K. D. Benkstein, J. van de Lagemaat, A. J. Frank, *J. Am. Chem. Soc.* **2003**, *125*, 6306; b) L. I. Halaoui, N. M. Abrams, T. E. Mallouk, *J. Phys. Chem. B* **2005**, *109*, 6334; c) I. Rodriguez, F. Ramiro-Manzano, P. Atienzar, J. M. Martinez, F. Meseguer, H. Garcia, A. Corma, *J. Mater. Chem.* **2007**, *17*, 3205.

[11] B. T. Holland, C. F. Blanford, A. Stein, *Science* **1998**, *281*, 538.

[12] Z. Cai, J. Teng, Z. Xiong, Y. Li, Q. Li, X. Lu, X. S. Zhao, *Langmuir* **2011**, *27*, 5157.

[13] J. W. Galusha, C.-K. Tsung, G. D. Stucky, M. H. Bartl, *Chem. Mater.* **2008**, *20*, 4925.

[14] H. Jiang, X. Yang, C. Chen, Y. Zhu, C. Li, *New J. Chem.* **2013**, *37*, 1578.

[15] a) Z. Y. Zhong, F. X. Chen, T. P. Ang, Y. F. Han, W. Q. Lim, A. Gedanken, *Inorg. Chem.* **2006**, *45*, 4619; b) S. H. Lim, J. Z. Luo, Z. Y. Zhong, W. Ji, J. Y. Lin, *Inorg. Chem.* **2005**, *44*, 4124.

[16] H. Li, L. Zhang, H. Dai, H. He, *Inorg. Chem.* **2009**, *48*, 4421.

[17] a) S. Bordere, P. L. Llewellyn, F. Rouquerol, J. Rouquerol, *Langmuir* **1998**, *14*, 4217; b) J.-X. Hu, H. Shang, J.-G. Wang, L. Luo, Q. Xiao, Y.-J. Zhong, W.-D. Zhu, *Ind. Eng. Chem. Res.* **2014**, *53*, 11828.

[18] H. W. Yan, C. F. Blanford, B. T. Holland, W. H. Smyrl, A. Stein, *Chem. Mater.* **2000**, *12*, 1134.

[19] J. Jeromenok, J. Weber, *Langmuir* **2013**, *29*, 12982.

[20] Q. Zhang, T. P. Chou, B. Russo, S. A. Jenekhe, G. Cao, *Adv. Funct. Mater.* **2008**, *18*, 1654.

[21] C. S. Rustomji, C. J. Frandsen, S. Jin, M. J. Tauber, *J. Phys. Chem. B* **2010**, 114, 14537.

[23] Y. H. Ko, G. S. R. Raju, S. Kim, J. S. Yu, *Phys. Status Solidi A* **2012**, *209*, 2161.

[24] a) K. Zhu, N. R. Neale, A. Miedaner, A. J. Frank, *Nano Lett.* **2007**, *7*, 69-74; b) K. Zhu,

T. B. Vinzant, N. R. Neale, A. J. Frank, *Nano Lett.* **2007**, *7*, 3739.
[25] L.-C. Du, Y.-X. Weng, *J. Phys. Chem. C* **2007**, *111*, 4567.
[26] G. Schlichthorl, N. G. Park, A. J. Frank, *J. Phys. Chem. B* **1999**, *103*, 782.
[27] K. Zhu, S.-R. Jang, A. J. Frank, *J. Phys. Chem. Lett.* **2011**, *2*, 1070.

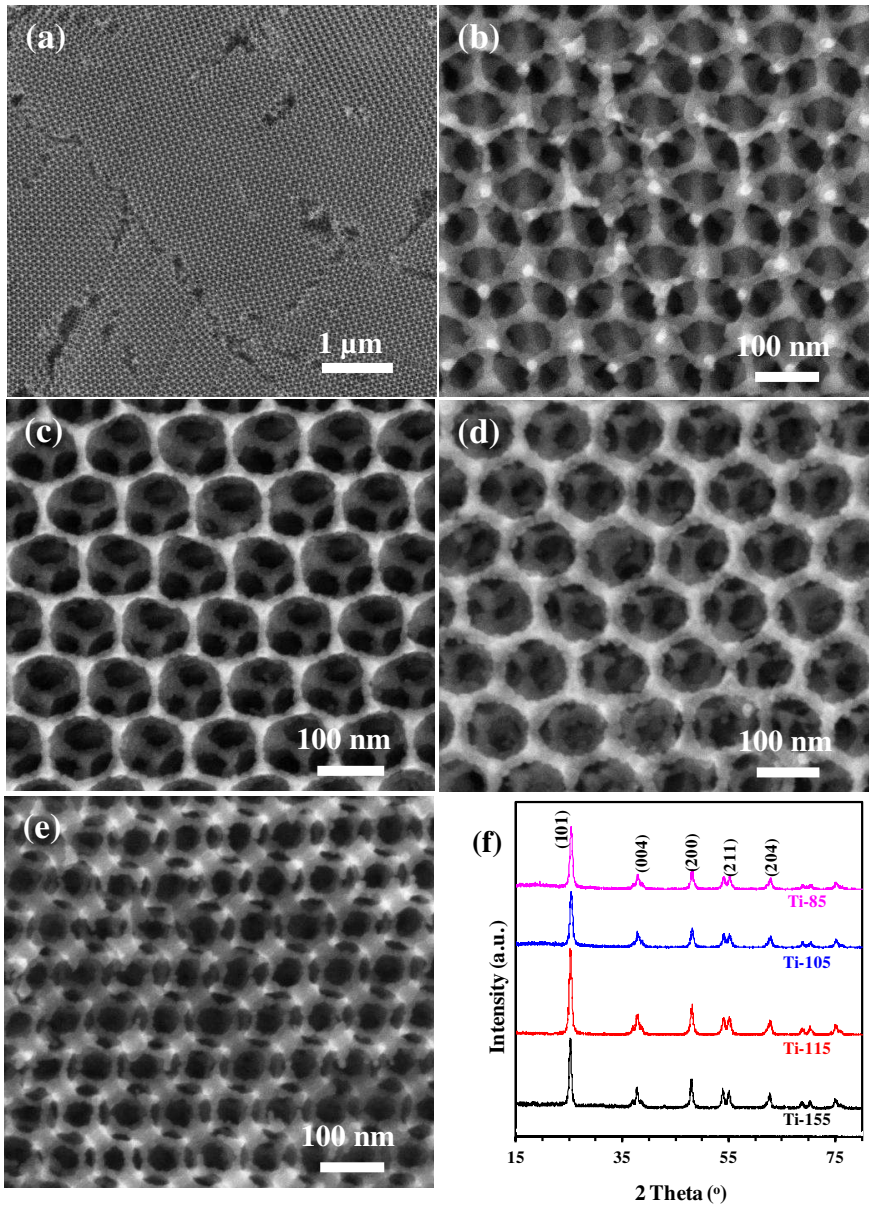

Figure 1. (a-e) SEM images of HS-3DOM TiO_2 samples: (a, b) Ti-155, (c) Ti-115, (d) Ti-105, and (e) Ti-85, as well as (f) their XRD patterns.

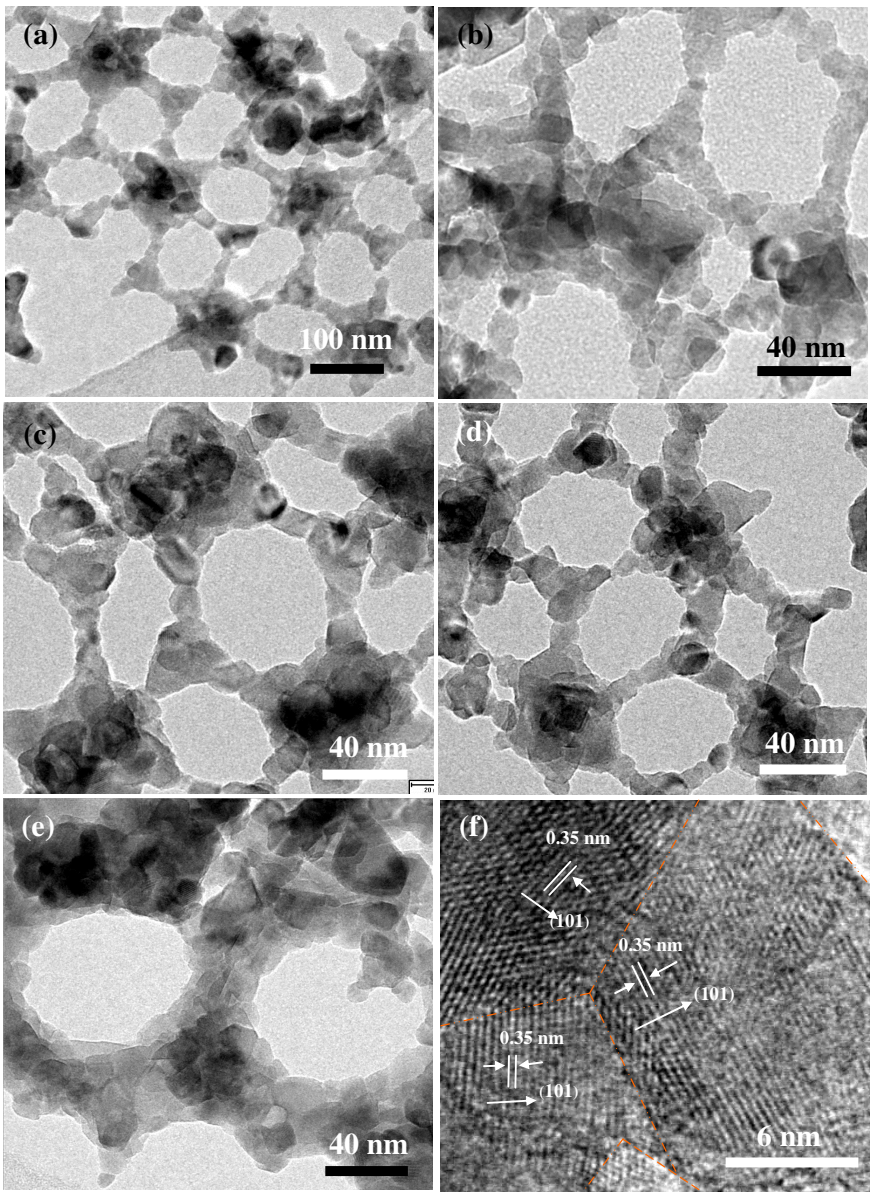

Figure 2. TEM images of (a,b) Ti-155, (c) Ti-115, (d) Ti-115, (e) Ti-85 samples and HR-TEM image shows *d*-spacing of the HS-3DOM TiO_2.

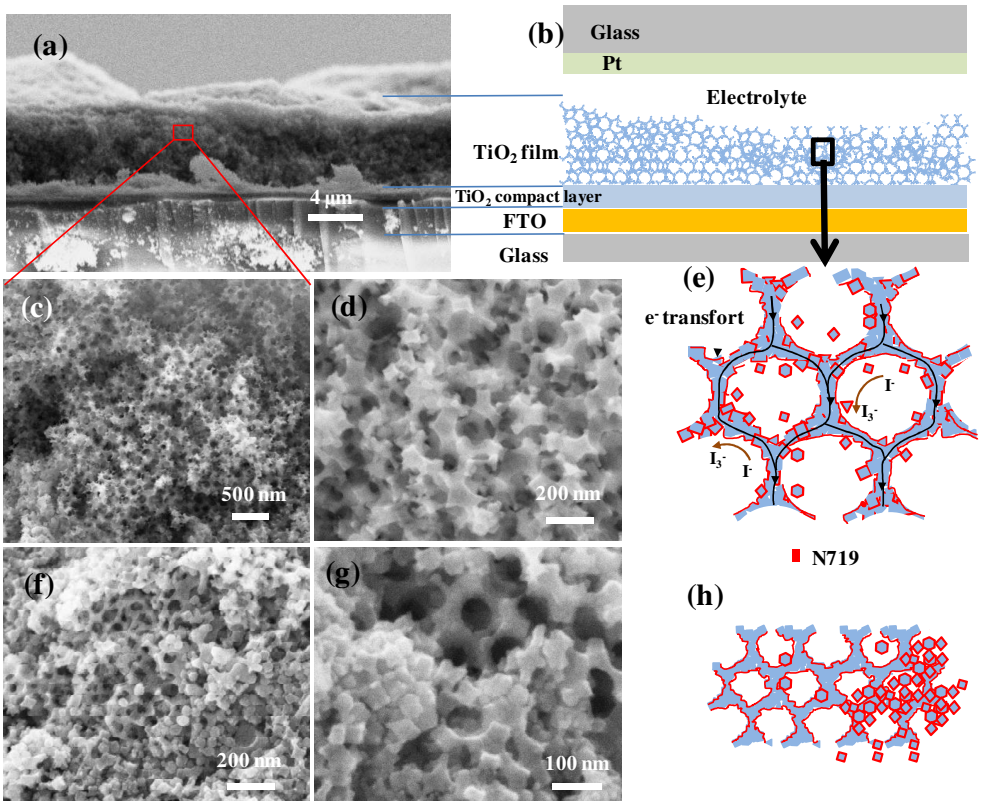

Figure 3. (a) Cross-sectional SEM image of Ti-155 film without dye loading, (b) Configuration of a full DSC-device based on HS-3DOM TiO2 in this study, high-resolution SEM imagies of (c,d) T-155, (f,g) Ti-85 layers and their structure illustrations of T-155 (e) and Ti-85(h) layers.

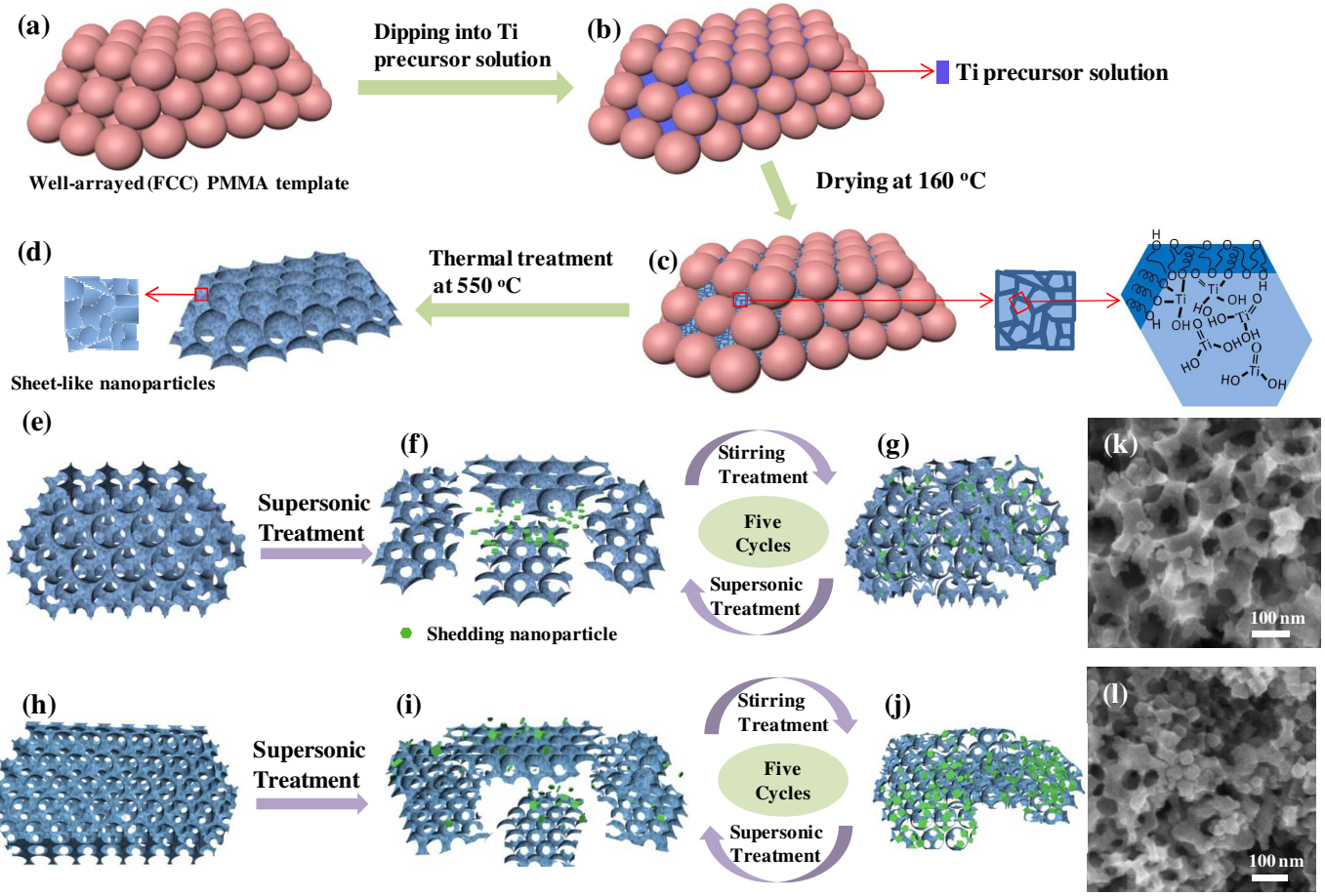

Figure 4. Schematic illustration of the paste formation process based on (a) Ti-155, Ti-155, and Ti-105 samples and the one based on (c) Ti-85 sample, as well as HR-SEM pictures of photoanode films based on (k) Ti-105 and (l) Ti-85 samples.

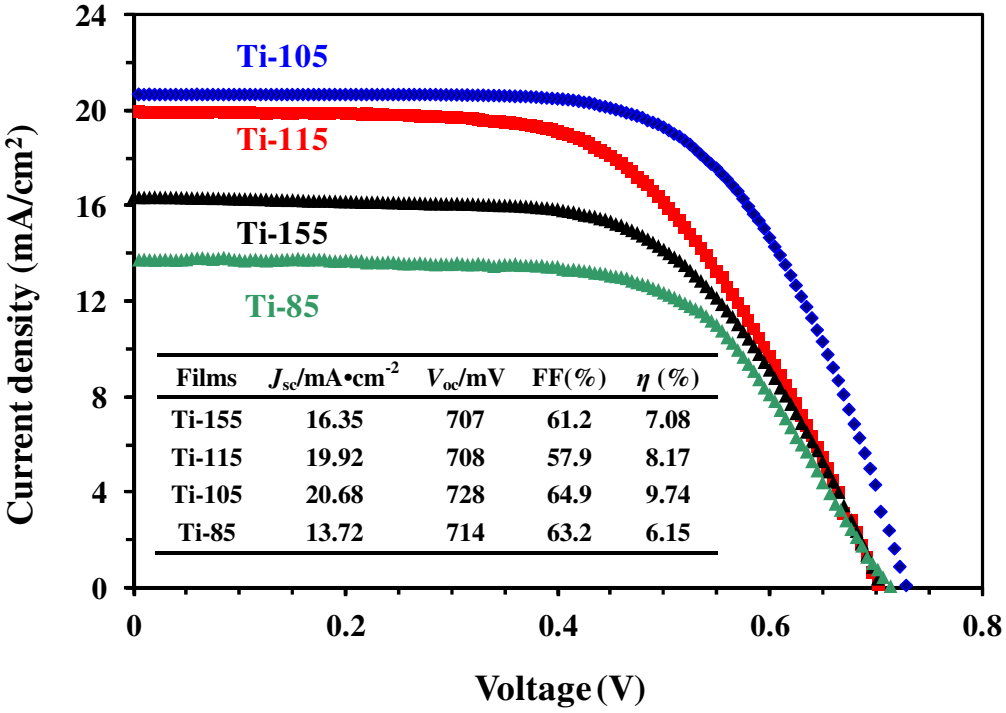

Films	J_{sc}/mA•cm^{-2}	V_{oc}/mV	FF(%)	η (%)
Ti-155	16.35	707	61.2	7.08
Ti-115	19.92	708	57.9	8.17
Ti-105	20.68	728	64.9	9.74
Ti-85	13.72	714	63.2	6.15

Figure 5. J-V curves of DSCs devices based on HS-3DOM TiO_2 with different macropore size and parameters of photovoltaic performance of DSCs devices based on three-dimensionally ordered hierarchically porous TiO_2 (insert).

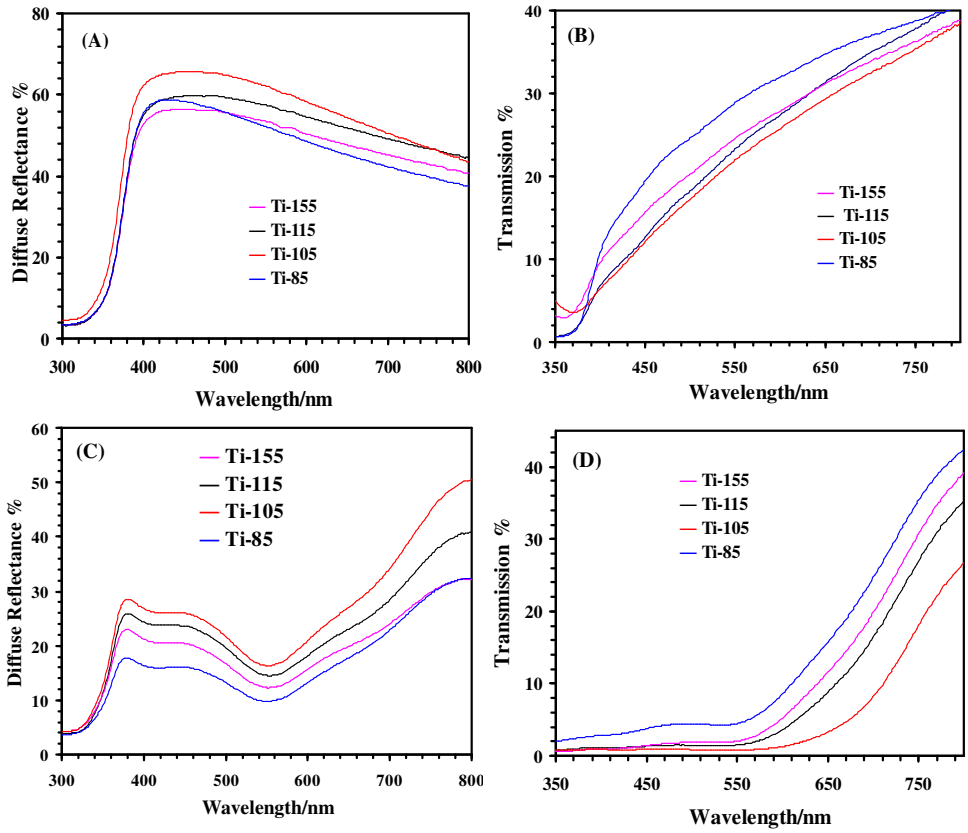

Figure 6. (A, C) Diffuse reflectance and (B, D) transmittance of porous TiO_2 layers based on HS-3DOM TiO_2 (A, B) without and (C, D) with N-719 sensitization.

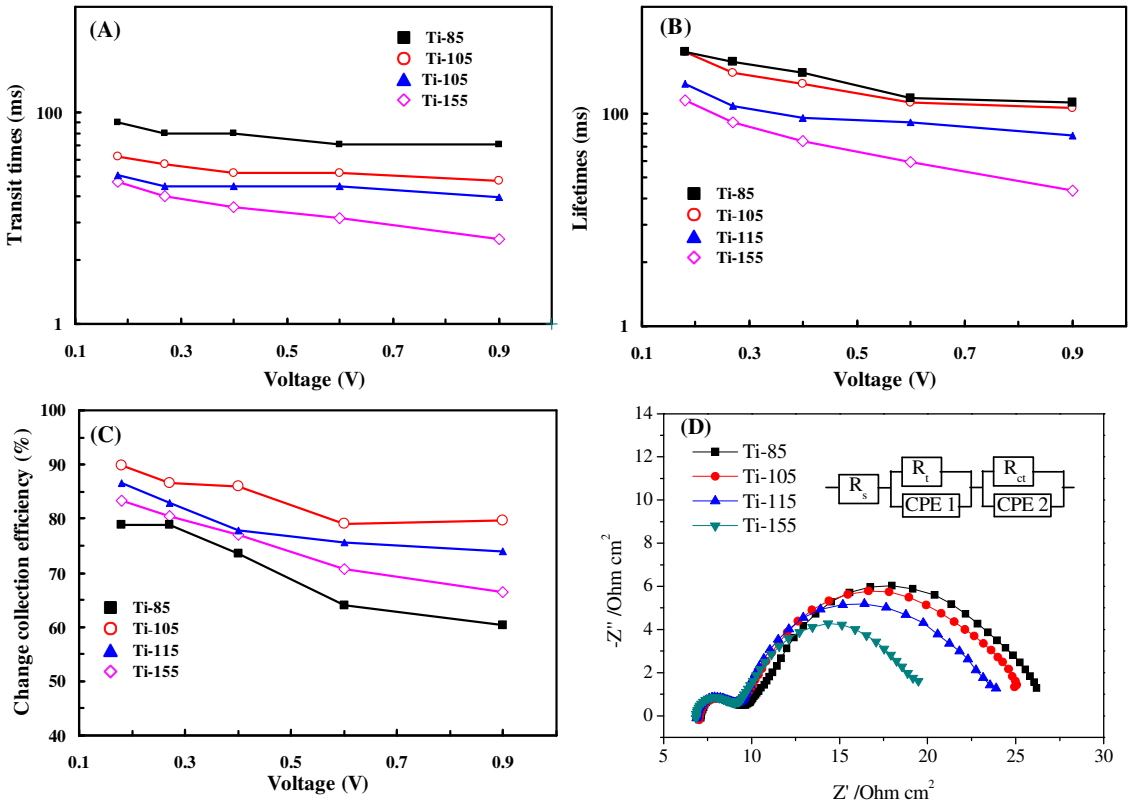

Figure 7 (A) electron transit times and (B) electron lifetime, (C) the charge collection efficiency measured by Intensity-modulated photocurrent/photovoltage spectroscopy (IMPS/IMVS) for cells based on Ti-155, Ti-115, Ti-105, and Ti-85, and (D) Nyquist plots of N719 dye-sensitized solar cells based on HR-3DOM TiO_2 under dark condition.

Table 1. texture parameters of photoanodes as-fabricated and their amount of adsorbed dye.

Device based on	a (m^2 g^{-1})	v_P (cm^3 g^{-1})	ρ/g cm^{-3}	A($\times 10^{17}$$nm^2$)	Idea amount of adsorbed dye (nmol cm^{-2})	Amount of adsorbed dye (nmol cm^{-2})
Ti-155	56.3	0.24	2.01	1.076	348.6	238
Ti-115	66.6	0.32	1.73	1.096	355.2	250
Ti-105	83.6	0.46	1.39	1.107	358.8	264
Ti-85	109.7	0.74	1.00	1.045	338.6	233

Table 2 Resistances of N719 dye-sensitized solar cells based on HR-3DOM TiO_2

Flims	R_s /Ω cm^2	Error /%	R_t /Ω cm^2	Error /%	R_{ct} /Ω cm^2	Error /%
Ti-155	6.87	0.76	2.39	3.96	10.97	1.86
Ti-115	6.92	1.23	2.61	5.72	13.72	2.11
Ti-105	7.05	1.04	2.34	5.21	16.17	1.38
Ti-85	7.12	1.36	2.45	5.54	16.55	1.99

Article type: Graphical abstract

Dye-Sensitized Solar Cells Based on Hierarchically Structured Porous TiO_2 Filled with Nanoparticles

*Zhenxuan Zhao [1], Guicheng Liu [1], Bo Li [2], Lixue Guo [1], Chengbin Fei [1], Yajie Wang [1], Lili Lv [2], Xiaoguang Liu [2], Jianjun Tian [1,2], Guozhong Cao *[1,3]*

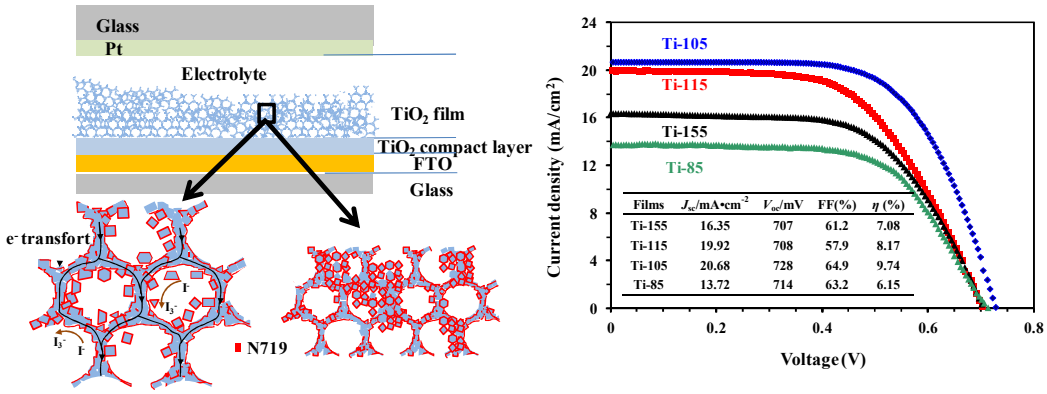

DSCs based on hierarchically structured porous TiO_2 filled with nanopartcles exhibited the highest PCE of 9.7%